Metal-Semiconductor Schottky Diodes with Record-High Rectification and Conductance Using Two-Dimensional Monolayer Decoration

Simran Shahi,[1] Maomao Liu,[1] Hemendra Nath Jaiswal,[1] Anindita Chakravarty,[1] Sichen Wei,[2] Yu Fu,[2] Asma Ahmed,[1] Anthony Cabanillas,[1] Fei Yao,[2]* and Huamin Li[1]*
[1]Department of Electrical Engineering, University at Buffalo, Buffalo, NY, USA
[2]Department of Materials Design and Innovation, University at Buffalo, Buffalo, NY, USA
*Email: feiyao@buffalo.edu, huaminli@buffalo.edu

2022 6th IEEE Electron Devices Technology & Manufacturing Conference (EDTM) | 978-1-6654-2178-2/22/$31.00 ©2022 IEEE | DOI: 10.1109/EDTM53872.2022.9798125

***Abstract*—**Two-dimensional (2D) materials are promising for next-generation energy-efficient nanoelectronics. In this work, we exploited sub-1-nm 2D monolayers ranging from semimetal to semiconductor and insulator to decorate metal-semiconductor (MS) interfaces and achieved an outstanding capacity of manipulating carrier injections through the 2D monolayers. A record-high rectification ratio (5.4×10^4) and conductance (2×10^5 S/m^2) were obtained from a Ti/MoS_2/p-Si/Al Schottky diode, which demonstrates the promising potential of the sub-1-nm 2D monolayers to boost the performance of various electron devices.

I. Introduction

With the rise of graphene (Gr), 2D materials have been extensively explored for energy-efficient nanoelectronics due to the natural quantum confinement in an atomically thin body [1, 2]. Especially for a stacking structure based on the 2D materials, the out-of-plane carrier transport through the 2D layered crystals plays a critical role for overall device performance [3-5]. In this work, we designed a novel metal/2D monolayer/semiconductor (M2DS) vertical structure, and tested it with different 2D monolayers (ranging from semimetal (*e.g.*, Gr) to semiconductor (*e.g.*, MoS_2) and insulator (*e.g.*, h-BN)) as well as different low and high work function metals (*e.g.*, Ti and Pd). Depending on the 2D monolayers, the carrier transport dominated by energy matching and barrier tunneling was discussed through a comprehensive and statistical analysis.

II. Device Fabrication and Measurement

The vertical-stacking M2DS Schottky diodes consist of top electrodes (Ti or Pd), 2D monolayers (Gr, MoS_2, or h-BN), p-Si substrate, and Al/Au bottom electrodes as shown in Fig. 1. First, the bottom-surface native oxides of the p-Si substrate (1-10 Ω·cm) were etched out using buffered oxide etchant (BOE, 6:1). Then the global Al/Au (50/30 nm) bottom electrode was deposited by electron-beam (e-beam) evaporation. Al was chosen as a dopant to provide Ohmic contact with the p-Si substrate. Then, the top-surface native oxides were etched out, followed by wet-transfer placement of the 2D monolayers synthesized by chemical vapor deposition (CVD) [6]. Next, the 100-nm-thick Ti and Au top electrode arrays (Ti/Au, 50/50 nm for Ti contact) were deposited by e-beam evaporation through a shadow mask. As a reference, the Ti- and Au-contact MS diodes without any 2D monolayer decoration were prepared through the same fabrication process. Therefore, the performance difference between the M2DS and MS diodes can be directly attributed to the introduction of 2D monolayer decoration at the MS interfaces.

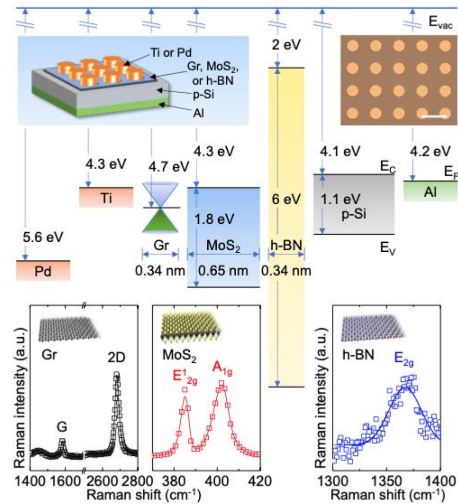

Fig. 1. Top panel: Device structure, microscopy image (scale bar: 300 μm), and energy band diagram of the M2DS diodes with 2D monolayer Gr, MoS_2, and h-BN decoration. Here E_{vac}, E_C, E_V, and E_F denote energy at the vacuum, conduction band minima, valence band maxima, and Fermi level, respectively. Bottom panel: Raman spectra of the 2D monolayer Gr, MoS_2, and h-BN.

III. Results and Discussion

A statistical characterization was carried out for 10 devices of each type of the M2DS diodes at room temperature, as shown in Fig. 2(a) and (b). Holes are considered as the majority charge carriers because of the p-Si involved in the M2DS structure. For $V_A < 0$ V, the hole injection is induced from the top electrode and

Authorized licensed use limited to: University at Buffalo Libraries. Downloaded on August 31,2022 at 12:19:15 UTC from IEEE Xplore. Restrictions apply.

governed by the M2DS interfacial barrier. Depending on the adapted 2D monolayers, the hole injection efficiency varies significantly for the Ti-contact M2DS diodes but becomes comparable for the Pd-contact ones. In comparison, for $V_A > 0$ V, both the Ti- and Pd-contact M2DS devices behave similarly, because the holes are injected through the identical Ti/p-Si interfaces from the bottom electrode. From the maximum J and G obtained at V_A = +/–20 V, it is found that the 2D monolayer decoration can significantly tune the carrier injection and thus J and G, depending on the metal selection. Taking the MoS_2 decoration as an example, the Ti-contact M2DS diodes can provide an ultrahigh rectification ratio of 5.4×10^4 which is ~5,000 higher than the referential device (~11).

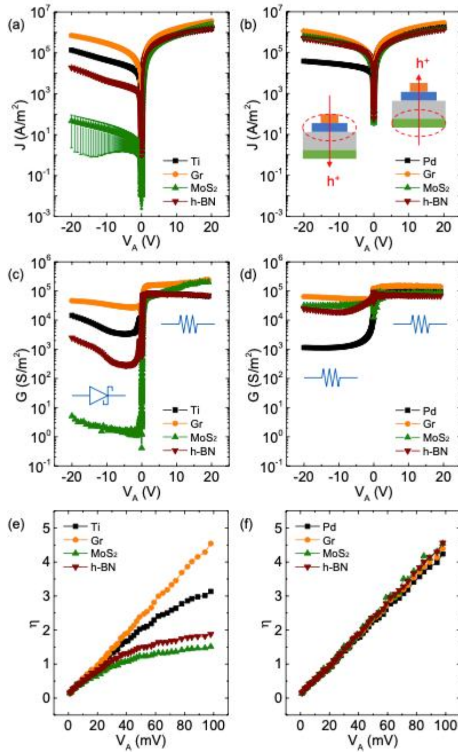

Fig. 2. Statistical characterizations including (a, b) J, (c, d) G, and (e, f) η as a function of V_A for the Ti- and Pd-contact M2DS diodes and the reference MS diodes. The holes are injected through the M2DS interfaces at $V_A < 0$ V.

The underlying mechanism of 2D monolayer decoration can be interpreted by their different thicknesses and bandgaps, as shown in Fig. 3. The semimetal Gr (0.34 nm) provides an energy matching at the MS interface and thus lowers the injection barrier [7, 8]. In contrast, the semiconducting MoS_2 (0.65 nm) and insulating h-BN (0.34 nm) with relatively large bandgaps introduce a quantum tunneling through the barriers, and the tunneling probability exponentially decays as the barrier thickness increases [9, 10].

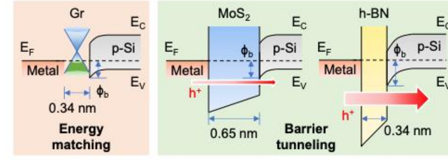

Fig. 3. The energy band diagram illustrates the carrier transport dominated by an energy matching for the Gr decoration and a barrier tunneling for the MoS_2 and h-BN decoration at the M2DS interfaces.

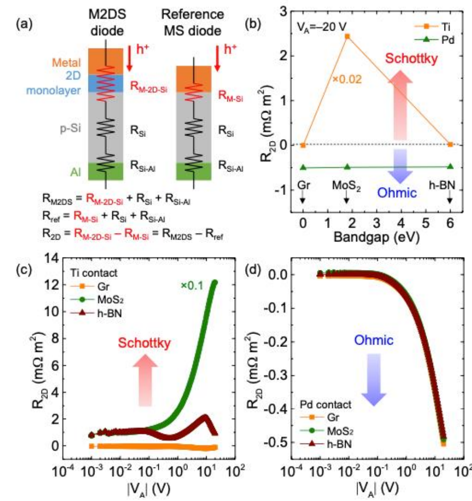

Fig. 4. Analysis of R_{2D} including (a) a model of resistors in series and (b-d) the dependence on the 2D monolayer bandgaps and negative V_A.

The impact of the 2D monolayer decoration can be quantitively visualized by a model of resistors in series, as shown in Fig. 4. The net resistance induced by the 2D monolayer decoration (R_{2D}) is extracted through a comparison between the M2DS diode and the reference MS diode. The positive R_{2D} promotes the Schottky contact with the higher rectification ratio, whereas the negative R_{2D} improves the Ohmic contact with the higher J and G. Such an outstanding tuning capability between the Schottky and Ohmic contacts exhibits the promising potential of the 2D monolayer decoration.

To further understand the carrier transport under the 2D monolayer decoration, a set of advanced characterizations are performed, as shown in Fig. 5. In the $\ln(J/V_A^2)$ versus $\ln(1/V_A)$ plots, the Gr decoration with good linearity indicates the dominance of direct tunneling (DT) and thermionic emission (TE) for both the Ti- and Pd-contact M2DS diodes. In comparison, the MoS_2 decoration is dominated by the DT and TE for the

Authorized licensed use limited to: University at Buffalo Libraries. Downloaded on August 31,2022 at 12:19:15 UTC from IEEE Xplore. Restrictions apply.

Pd-contact M2DS devices, but is governed by Fowler-Nordheim tunneling (FNT) for the Ti-contact M2DS devices. Therefore, for the Ti-contact M2DS diodes, the decay of R_{2D} with the MoS_2 decoration can be attributed to the FNT, and a similar DT-to-FNT transition for the case of h-BN decoration can be anticipated as V_A continues increasing.

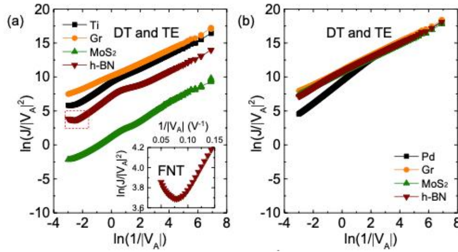

Fig. 5. Carrier transport characterizations in the M2DS diodes and the reference MS diodes.

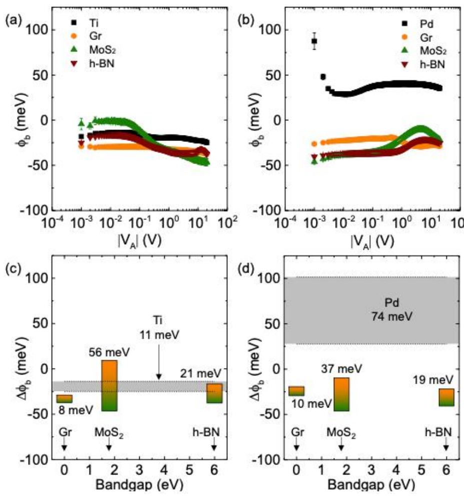

Fig. 6. The extracted ϕ_b for various M2DS diodes and the reference MS diodes, including (a, b) ϕ_b as a function of the negative VA and (c, d) $\Delta\ \phi_b$ as a function of the 2D monolayer bandgaps.

Using a temperature-variable (130 to 300 K) measurement, Schottky barrier height (ϕ_b) as a function of V_A is extracted from the Arrhenius plots [10-13], as shown in Fig. 6. Compared to the reference devices, the Ti-contact MoS_2 decoration has the largest ϕ_b variation ($\Delta\phi_b$) which contributes to a strong current rectification. Whereas all of the Pd-contact 2D monolayer decorations exhibit a much smaller $\Delta\phi_b$, leading to an Ohmic-like contact condition.

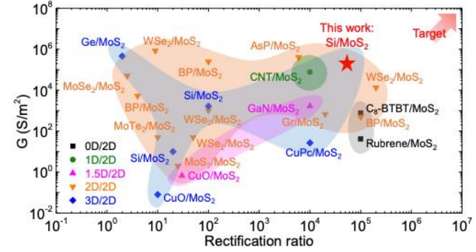

Fig. 7. Benchmarking of the Ti-contact MoS_2-decorated M2DS diodes with other state-of-the-art MoS_2-based vertical-junction diodes.

Finally, the rectification ratio and G of the Ti-contact M2DS diodes with the MoS_2 decoration are selected to benchmark with other state-of-the-art MoS_2-based vertical-junction diodes composed of multi-dimensional materials [12, 14-34], as shown in Fig. 7. Our device possesses a record-high performance, suggesting the great potential of the 2D monolayer decoration for next-generation electron devices.

IV. Conclusion

We demonstrated a record-high rectification ratio and G from the M2DS diodes. The sub-1-nm 2D monolayer decoration at the MS interfaces can effectively manipulate the carrier transport with a large tuning range and boost the performance of various electron devices.

Acknowledgment

The authors acknowledge support from the National Science Foundation (NSF) under Award ECCS-1944095, the New York State Energy Research and Development Authority (NYSERDA) under Award 138126, the New York State Center of Excellence in Materials Informatics (CMI), and the Vice President for Research and Economic Development (VPRED) at the University at Buffalo.

References [1] *Nat. Mater.*, 6, 183, 2007. [2] *Nat. Nanotech.*, 9, 768, 2014. [3] *Nature*, 499, 419, 2013. [4] *Science*, 353, aac9439, 2016. [5] *Nat. Rev. Mater.*, 1, 16042, 2016. [6] *Nanotechnology*, 28, 36LT01, 2017. [7] *IEEE Electron Dev. Lett.*, 35, 599, 2014. [8] *Nano Lett.*, 15, 3030, 2015. [9] *Adv. Mater.*, 28, 8302, 2016. [10] *Adv. Mater.*, 32, 2002716, 2020. [11] *Sci. Rep.*, 4, 4041, 2014. [12] *Nat. Commun.*, 6, 6564, 2015. [13] *Nanoscale*, 12, 17253, 2020. [14] *Adv. Funct. Mater.*, 25, 5865, 2015. [15] *Appl. Phys. Lett.*, 107, 183103, 2015. [16] *PNAS*, 110, 18076, 2013. [17] *Adv. Electron. Mater.*, 5, 1800976, 2019. [18] *ACS Nano*, 10, 7451, 2016. [19] *Nano Lett.*, 14, 4785, 2014. [20] *ACS Nano*, 8, 8292, 2014. [21] *ACS Nano*, 10, 3852, 2016. [22] *ACS Appl. Mater. Interfaces*, 10, 37258, 2018. [23] *Nat. Commun.*, 10, 4664, 2019. [24] *Nano Lett.*, 14, 5590, 2014. [25] *Nano Lett.*, 20, 3651, 2020. [26] *ACS Nano*, 9, 2071, 2015. [27] *Nano Lett.*, 16, 1359, 2016. [28] *ACS Nano*, 11, 9143, 2017. [29] *Nano Res.*, 13, 1053, 2020. [30] *Mater. Horiz.*, 4, 274, 2017. [31] *Nanoscale*, 7, 15442, 2015. [32] *ACS Nano*, 8, 3042, 2014. [33] *Sci. Rep.*, 4, 5458, 2014. [34] *Nature*, 526, 91, 2015.

Authorized licensed use limited to: University at Buffalo Libraries. Downloaded on August 31,2022 at 12:19:15 UTC from IEEE Xplore. Restrictions apply.